Applied Surface Science 479 (2019) 626–633

Contents lists available at ScienceDirect

Applied Surface Science

journal homepage: www.elsevier.com/locate/apsusc

Full length article

Transition metal substitution on Mg(10$\bar{1}$3) and Mg(0001) surfaces for improved hydrogenation and dehydrogenation: A systematic first-principles study

Jia-Jun Tang[a,b,*], Jia-Hui Ye[a], Yan-Xiong Fang[a], Zhan Lin[a], Yu-Jun Zhao[b,**]

[a] School of Chemical Engineering and Light Industry, Guangdong University of Technology, Guangzhou 510006, PR China
[b] Department of Physics, South China University of Technology, Guangzhou 510640, PR China

ARTICLE INFO

Keywords:
Mg
Hydrogen storage
Low-index and high-index surface
Transition metal
Low temperature
First-principles

ABSTRACT

The experimentally prepared high-index Mg(10$\bar{1}$3) is able to lower the H adsorption temperature by 200 K. The potential of hydrogen sorption properties of high-index Mg(10$\bar{1}$3) deserves further investigations. In this paper, we conduct first-principles calculations to study the stabilities of transition metal substitution on the conventional low-index Mg(0001) and the experimentally prepared high-index Mg(10$\bar{1}$3), including Sc, Ti, V, Cr, Mn, Fe, Co, Ni, Cu, Zn, Y, Zr, Nb, Mo, Tc, Ru, Rh, Pd, Ag, Cd, Pt and Au. Our results show that Mg(10$\bar{1}$3) can stabilize Ni, Zn, Ag, Cd and Au on the outermost layer, while, on Mg(0001), all the TM dopants studied have a lower stability on the outermost layer except Cd than the second outermost layer. This difference is because of charge depletion and charge smoothing effects more obvious in the surface regions of high-index surface. Consequently, substituted TMs on Mg(10$\bar{1}$3) exhibit larger atomic displacements toward the bulk region along *z* axis in order to form bonds with neighboring Mg atoms. Substituted TMs on Mg(10$\bar{1}$3) form stronger TM-H bonds compared to Mg(0001). For H_2 dissociation, Ni and Zn are capable of dramatically lowering the energy barrier of H_2 dissociation from 0.90 eV on pure Mg(0001) surface to 0.02 eV on Ni/Mg(10$\bar{1}$3) and to 0.39 eV on Zn/Mg(10$\bar{1}$3). For H_2 formation, Ni/Mg(10$\bar{1}$3) and Zn/Mg(10$\bar{1}$3) have energy barriers of 0.41 eV and 0.42 eV, respectively, slightly larger than the pure Mg(10$\bar{1}$3) of 0.39 eV. In summary, our thermodynamics and kinetics results imply that Ni- and Zn-substituted high-index Mg(10$\bar{1}$3) can be a promising material for hydrogen storage, and open the gate for digging the hydrogen sorption property potential of TM-doped high-index surface.

1. Introduction

The utilization of H energy, an environmentally friendly source of energy, has aroused a heated research trend at the global scale [1,2], such as water splitting [3] and hydrogen storage [4]. Hydrogen-rich compounds are used for hydrogen storage medium, but the poor reversibility hinders its commercial application [5].

Magnesium, a promising hydrogen storage material candidate, has been extensively studied in the past decade because of its safety, high and reversible storage capacity of 7.6 wt% and low cost [6,7]. However, the slow kinetics of H sorption and the recycle stability of Mg-based materials become the bottleneck for the practical application, resulting in a high operation temperature above 300 °C [8]. Numerous efforts have attempted to overcome the obstacles. For example, on the one hand, attempts to alloy the Mg material with transition metals (TMs) have been made, such as Cu-/Ti-/Ni-/Y-Mg binary materials [9–12], and Y-In-/Y-Ni-/Y-Zn-/Y-La-/Pr-Y-/Ti-Ni-Mg ternary materials [13–16]. The alloys change the property of surface as well as the bulk, facilitating the H dissociation and diffusion and promoting the cycling stability. On the other hand, surface or bulk modifications have also been made to improve the H storage performance of Mg. Nano-crystalline Mg can increase the specific surface area thus achieving lower-enthalpy adsorption by transferring excess surface energy to formation heat [8,17]. Mixing the γ-MgH_2 and β-MgH_2 could also reduce the H desorption temperature to 200 °C and the readsorption one to 100 °C [18]. Our previous work [19] has found that the high index Mg(10$\bar{1}$3) slab could significantly reduce the adsorption temperature from 300 °C to 119 °C while the density functional theory (DFT) calculations also point out that the H is more energetically favorable to fast diffuse along the close-packed planes, and the H diffusion into bulk region exhibits an energy barrier much lower than that on the Mg(0001) slab.

Substantial studies reveal the mechanism of capacity reduction

* Correspondence to: J.-J. Tang, School of Chemical Engineering and Light Industry, Guangdong University of Technology, Guangzhou 510006, PR China.
** Corresponding author.
E-mail addresses: pcntsfad@gmail.com (J.-J. Tang), zhaoyj@scut.edu.cn (Y.-J. Zhao).

https://doi.org/10.1016/j.apsusc.2019.02.124
Received 6 December 2018; Received in revised form 11 January 2019; Accepted 14 February 2019
Available online 15 February 2019
0169-4332/

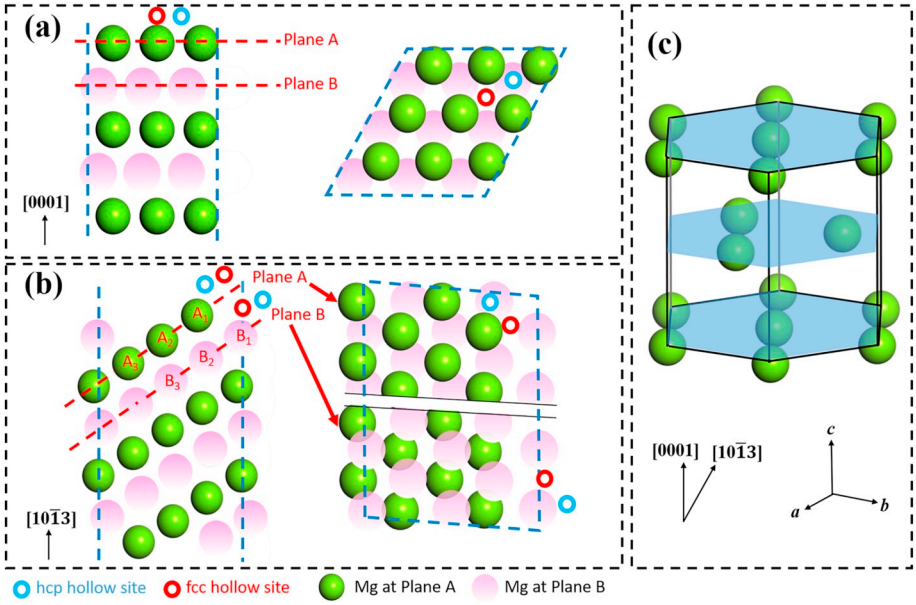

Fig. 1. Arrangement and three-fold hollow sites of (a) Mg(0001) and (b) Mg(10$\bar{1}$3) surfaces, and (c) the diagram of Mg close-packed plane (the close-packed plane is vertical to the principle *c*-axis).

Table 1
Comparison of the most stable substitution site for the TM (Sc, Ti, V, Cr, Mn, Fe, Co, Ni, Cu, Zn, Y, Zr, Nb, Mo, Tc, Ru, Rh, Pd, Ag, Cd, Pt, Au) substituted at Mg (0001) and Mg(10$\bar{1}$3) surface.

Substituted metal	Mg(0001)		Mg(10$\bar{1}$3)	
	Most stable site	E_{sub} (eV)	Most stable site	E_{sub} (eV)
Sc	Plane B	−0.05	B_2	−0.13
Ti	Plane B	0.79	B_2	0.59
V	Plane B	1.29	B_2	1.13
Cr	Plane B	1.10	B_2	1.02
Mn	Plane B	0.74	B_2	0.62
Fe	Plane B	1.15	B_2	0.88
Co	Plane B	0.41	B_2	0.00
Ni	Plane B	0.28	A_1	−0.03
Cu	Plane B	0.24	A_1	0.02
Zn	Plane B	0.07	A_1	−0.03
Y	Plane B	−0.12	B_3	−0.17
Zr	Plane B	0.41	B_2	0.21
Nb	Plane B	1.33	B_2	1.01
Mo	Plane B	1.87	B_2	1.47
Tc	Plane B	1.22	B_2	0.74
Ru	Plane B	0.41	B_2	−0.08
Rh	Plane B	−0.86	B_2	−1.24
Pd	Plane B	−1.25	B_2	−1.45
Ag	Plane B	−0.41	A_1	−0.50
Cd	Plane A	−0.28	A_1	−0.30
Pt	Plane B	−1.63	B_2	−1.92
Au	Plane B	−1.20	A_1	−1.40

during H uptake and release. The hydrogen uptake and release processes can be complicated, involving H_2 dissociation, H diffusion, phase transformation and H_2 formation and desorption [8]. There are inevitably the atomic rearrangements or reconstructions at high temperature. For instance, γ-MgH_2 phase disappears after five cycles of H uptake [18]. Meanwhile, the restructuring of the Mg-based alloy would also cause the reduction on hydrogen capacity, such as Y-Ni-Mg alloy [15], Co-Mg [20], Fe-Mg [21], Ti-Mg and Ni-Mg [16]. Thus, the phase/surface stability is worth being concerned, and a low working temperature can be ideal for preventing surface reconstruction. Interestingly, theoretical calculations show that the doped TMs which strengthen H adsorption are more stable inside the bulk than on the surface [22,23]. The ways of increasing the stability of TMs in surface region are considered to be able to improve surface H sorption properties. A stable Mg-based material for hydrogen storage can be one: (i) that avoids high working temperature; (ii) that retains thermodynamic stability of the transition metals on the surface; (iii) that is capable of promoting H_2 uptake and release, and effectively transferring H into the bulk. Considering the fact that Mg(10$\bar{1}$3) slab has experimentally shown [19] its effective lowering of working temperature and its facilitation of fast H_2 uptake and release, we deem it is worthy to theoretically research the thermodynamic stability of TMs in the surface and dig the potential of TM-catalyzed H diffusion along the close-packed plane on the high-index surface, which may further experimentally decrease the working temperature of H sorption. Necessary comparisons with the low-index Mg(0001) surface are also illuminating. From the dimension of Mg(0001) surface, numerous calculation works instituted the magnesium hydroxide system to a satisfactory. The well-established system contains H_2 dissociation [24–29], H adsorption [30–32], H diffusion [29,32,33], stress/strain and Friedel oscillation effect [32,34–37] as well as the properties of transition metal doped Mg(0001) [22,23,38–43]. The high H_2 dissociation barrier (~0.87 eV) over Mg (0001), much higher than the diffusion barrier of 0.48 eV, together with the "blocking effect" [44] dominate the slow hydrogen kinetic sorption, whereas the Cu, Pd, Ni, Rh, Co Ru Fe, Zr and Ti doped Mg(0001) were predicted to improve the dissociation process. Although these transition metals significantly decrease the H_2 dissociation barrier, the stabilities of the surface are usually neglected, which might result in the deviation to the application.

In this report, we systematically compare the various TM-substituted (Sc, Ti, V, Cr, Mn, Fe, Co, Ni, Cu, Zn, Y, Zr, Nb, Mo, Tc, Ru, Rh, Pd, Ag, Cd, Pt, Au) Mg(0001) and Mg(10$\bar{1}$3) surface by employing ab initio calculations. In the first part, we calculate the TM substitutional energies on various sites and compare their relative stabilities to identify the preferred substitution sites on these two surfaces. These outcomes are explained from the surface charge distribution perspective. In the second part, H adsorption energies on the pure high-index Mg(10$\bar{1}$3) and TM-substituted Mg(10$\bar{1}$3) surfaces (i.e., TM substituted on the outermost layer) are calculated and the differences of adsorption energies and bond lengths are introduced to evaluate the factors that impact the TM-substituted Mg surface stability. Furthermore, by considering TM-substituted surface stability, TM-H interaction and metal availability, Ni and Zn are calculated to be the representatives and related H_2 dissociation and formation barriers are calculated. Lastly, the

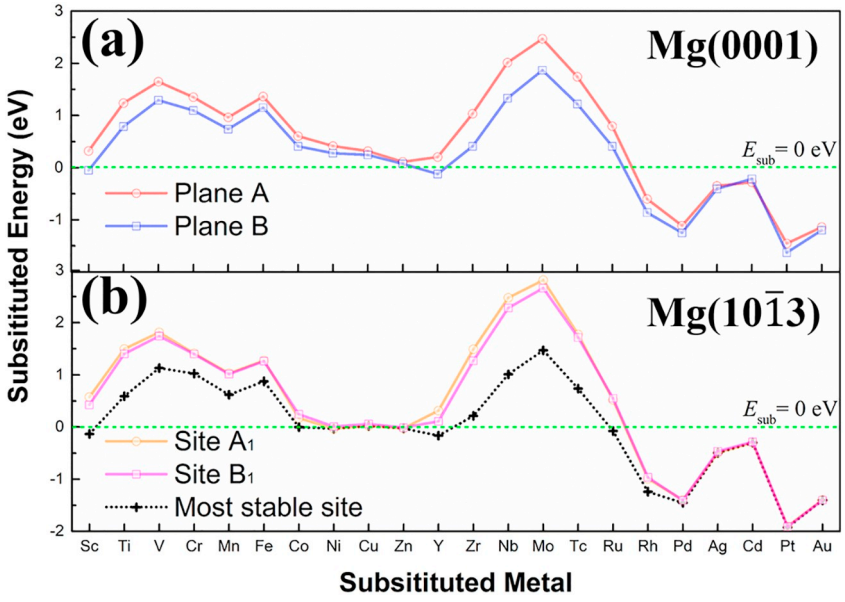

Fig. 2. The substitutional energies (E_{sub}) of the transition metals at (a) the Plane A and Plane B of Mg(0001) and (b) the A_1 and B_1 sites of Mg(10$\bar{1}$3) surface. The green lines represent the value of E_{sub} = 0 eV, whereas the black line depicted in (b) indicates the lowest E_{sub} of the specified metal located at the six sites of A_1, A_2, A_3, B_1, B_2 or B_3.

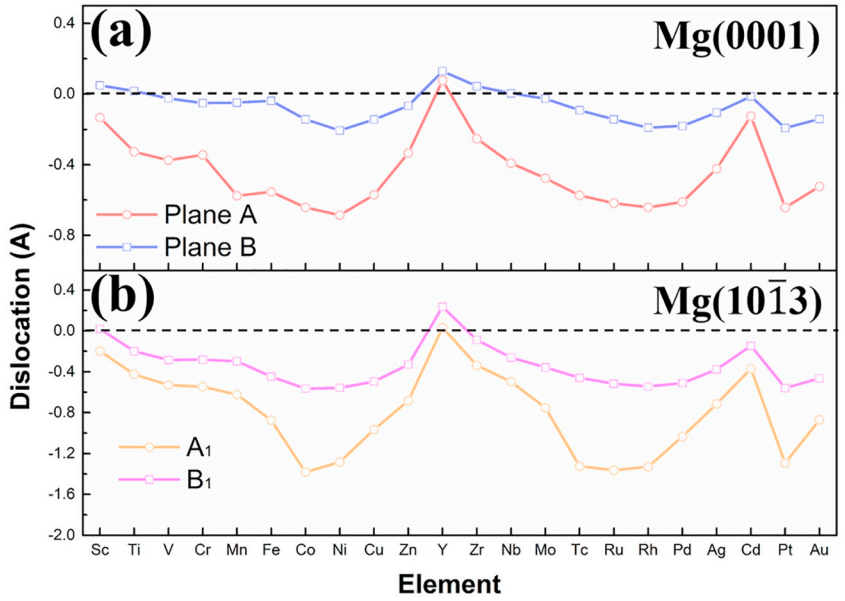

Fig. 3. The dislocation of the transition metals along *z* direction with respect to the substituted Mg position on the (a) Mg(0001) and (b) Mg(10$\bar{1}$3) surface.

conclusions are presented.

2. Computational methodology

DFT calculations are performed using Vienna ab initio simulation package (VASP) [45], while the electron-ion interactions are described with a plane-wave DFT code using generalized-gradient approximation (GGA) and projector augmented wave (PAW) [46–48]. For each model, the hexagonal close-packed (hcp) bulk Mg is employed with the calculated lattice constants of $a = b = 3.19$ Å, $c = 5.17$ Å with the c/a ratio of 1.62 and an included angle of 120° between a and b axes, and a cohesive energy of 1.52 eV/Mg atom. The calculated lattice constants are consistent with the experimental values ($a = 3.21$ Å, $c/a = 1.62$ and a cohesive energy of 1.51 eV/atom) [49,50].

For the Mg(0001) surface, a five-layer (3 × 3) slab was modeled, while each slab was separated by a 12 Å vacuum. The Mg(10$\bar{1}$3) surface is constructed using a (2 × 4) supercell of eleven Mg atomic layers. Every layer contains 4 Mg atoms, and the vacuum thickness between slabs is set to 12 Å. The non-equivalent positions of Mg are substituted by a TM atom in the order of Sc, Ti, V, Cr, Mn, Fe, Co, Ni, Cu, Zn Y, Zr, Nb, Mo, Tc, Ru, Rh, Pd, Ag, Cd, Pt, Au. All the simulations are carried out by immobilizing the bottom two Mg layers, and the Brillouin zone is sampled with a 3 × 3 × 1 k-mesh [51]. The TM dopant concentrations on Mg(0001) and Mg(10$\bar{1}$3) are 11%, 13% in the surface region (i.e., for the atoms allowed to move) and 2%, 1% to the bulk (i.e., for the whole model), respectively. The energy cutoff is 400 eV. Spin-polarized calculations are considered in all cases. The energies and total forces convergence criteria for structural optimizations are below 1×10^{-3} eV and 0.02 eV/Å.

The structural stability of TM-substituted Mg surface is defined as Eq. (1) shown below

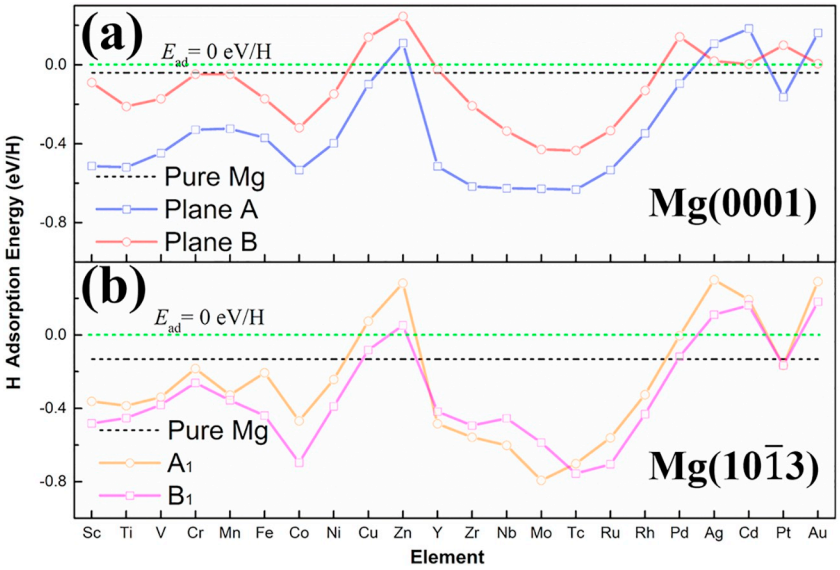

Fig. 4. H adsorption energies on TM-substituted (a) Mg(0001) and (b) Mg(10$\bar{1}$3) surface. The red and blue lines correspond to the cases of TM-substituted Mg(0001) on Plane A and Plane B, while the orange and purple ones are related to the TM-substituted Mg(10$\bar{1}$3) at Site A_1 and B_1. The black lines correspond to the adsorption energy of H adsorbed on (a) Plane A of pure Mg(0001) and (b) A_1 of pure Mg(10$\bar{1}$3).

Table 2
Comparison of the bond lengths of TM-H (Sc, Ti, V, Cr, Mn, Fe, Co, Ni, Cu, Zn, Y, Zr, Nb, Mo, Tc, Ru, Rh, Pd, Ag, Cd, Pt, Au) on Mg(0001) and Mg(10$\bar{1}$3) surfaces.

Substituted metal	Radii [55]	Mg(0001)	Mg(10$\bar{1}$3)	
	(Å)	Plane A (Å)	A_1 (Å)	B_1 (Å)
Mg	1.60	2.01	1.90	1.94
Sc	1.64	2.02	1.98	1.97
Ti	1.47	1.89	1.90	1.87
V	1.35	1.83	1.83	1.81
Cr	1.30	1.80	1.78	1.75
Mn	1.35	1.67	1.63	1.63
Fe	1.26	1.67	1.58	1.63
Co	1.25	1.57	1.55	1.56
Ni	1.25	1.58	1.56	1.57
Cu	1.28	1.67	1.63	1.63
Zn	1.37	1.83	1.76	1.71
Y	1.80	2.15	2.14	2.13
Zr	1.57	2.01	2.00	2.00
Nb	1.41	1.90	1.91	1.90
Mo	1.36	1.82	1.80	1.80
Tc	1.30	1.74	1.71	1.73
Ru	1.33	1.70	1.67	1.68
Rh	1.34	1.69	1.66	1.66
Pd	1.38	1.75	1.71	1.76
Ag	1.44	1.96	1.92	1.85
Cd	1.49	3.18	2.85	1.94
Pt	1.38	1.68	1.67	1.65
Au	1.44	1.85	1.78	1.77

$$E_{sub} = E_{TM/Mg} + E_{Mg-bulk} - E_{TM} - E_{Mg} \quad (1)$$

where $E_{TM/Mg}$ and E_{Mg} stand for the total energies of the TM-substitute Mg surface and pure Mg(0001) or Mg(10$\bar{1}$3) surface, while $E_{Mg\text{-}bulk}$ and E_M represent the energy of per atom in the bulk structure of Mg and TM. The configuration with a negative E_{sub} is stable.

The average adsorption energy ($E_{M/ad}$) per hydrogen on TM-substituted Mg surface is calculated by Eq. (2).

$$E_{TM/ad} = \frac{1}{N_H}\left[E_{TM/MgH} - \left(E_{TM/Mg} + \frac{N_H}{2}E_{H_2}\right)\right] \quad (2)$$

In the formula, $E_{TM/MgH}$ is the total energy of TM/Mg-H system. The more negative $E_{TM/ad}$ is, the more stable the structure is.

The energy barriers for H_2 dissociation are estimated using the climbing image nudged elastic band (CI-NEB) method in VASP [52]. A five-layered (2 × 2) Mg(0001) model and a six-layered (2 × 2) Mg(10$\bar{1}$3) model are modeled. At least five images are adopted in the NEB calculations to perform for gaining the minimum energy pathway and energy barrier for all designed diffusion routes. The Monkhorst-Pack *k*-point grids is set to (3 × 3 × 1) of Mg(0001) and (5 × 3 × 1) of Mg(10$\bar{1}$3), whereas the energies and total forces convergence criteria for all the atoms of images are below 1×10^{-3} eV and 0.03 eV/Å.

3. Results and discussions

3.1. Stability of the TM-substituted Mg surface

The bulk structural properties, lattice constants and cohesive energies, of the pure transition metals are calculated, which are consistent with the previous finding (Table S1) [22,53]. As shown in Fig. 1, Mg (0001) and Mg(10$\bar{1}$3) surfaces are built with two types of non-equivalent planes labeled Plane A and Plane B. One TM atom replaces an Mg atom located at two topmost layers (Plane A and Plane B) of Mg(0001) and three topmost layers of Mg(10$\bar{1}$3) (A_1, A_2, A_3, B_1, B_2 and B_3). As shown in Fig. 1(c), the close-packed plane of Mg(0001) surface is perpendicular to *c*-axis.

Here, we mainly consider the specified TM atoms replace the Mg atom rather than TM doping at the interstitial position, which causes systemic distortion as well as instability [23]. Consequently, the stabilities of TM-substituted Mg surfaces are considered. Tables S2 and S3 list the total energies of the TM- substituted Mg(0001) and Mg(10$\bar{1}$3) surface. Fig. 1 shows the variations of E_{sub} according the periodic sequence of the transition metals. The trend and values of E_{sub} of Mg (0001) are consistent with the pervious study [22]. A similar periodic tendency of E_{sub} can be observed on Mg(10$\bar{1}$3).

The substitutional energies and the most energetically preferred substitution sites on the two surfaces are summarized in Table 1. It can be observed that, in Fig. 2, on both surfaces most TMs prefer the substitution on the inner planes than the outermost one, as manifested by the more positive numbers of the red line in Fig. 2(a) and the orange line in Fig. 2(b). This is understandable. Our previous study [37] has found charge depletion occurs in Mg surface region and charge transfer to the inner bulk region is obvious. The charge depletion caused by undercoordinated Mg atoms is the dominating factor affecting the

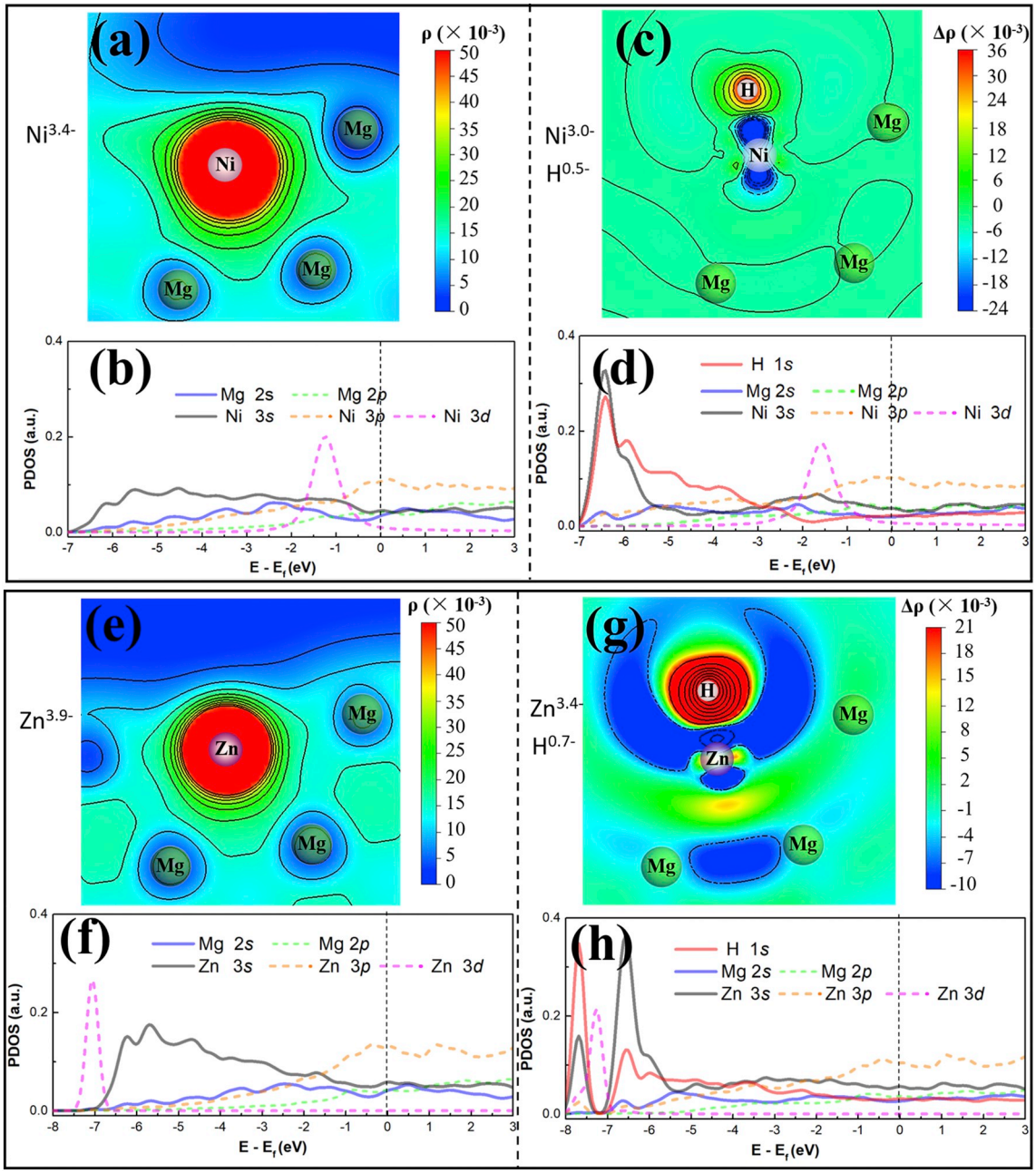

Fig. 5. (a) The charge density on Ni/Mg(10$\bar{1}$3) and (b) the charge density difference of H adsorbed Ni/Mg(10$\bar{1}$3) with respective PDOS of (c) Mg and Ni, and (d) H, Mg and Ni; and (e) the charge density on Zn/Mg(10$\bar{1}$3) and (f) the charge density difference of H adsorbed Zn/Mg Mg(10$\bar{1}$3) with respective PDOS of (g) Mg and Ni, and (h) H, Mg and Zn. The black dashed lines in PDOS figures represent the Fermi level in the systems.

atomic relaxations along *z* direction. In other words, for both low-index Mg(0001) surface and Mg(10$\bar{1}$3) surface, the charge density is higher in the inner surface than on the outermost surface. Importantly, the charge density difference between the first and the second outermost layers on Mg(10$\bar{1}$3) is larger than that on Mg(0001). Thus, when a pure Mg(10$\bar{1}$3) surface is created by cutting Mg—Mg bonds from Mg bulk, the Mg atom relaxation toward the bulk can be observed to be more obvious. For the TMs the electronegativities of which are generally higher than Mg, they naturally prefer the inner surface substitution. As shown in Fig. 3, we observe that the TMs with higher electronegativity have large dislocation along *z* direction, more easily forming bonds with neighboring Mg atoms. For example, Co, Ni, Tc, Ru and Rh have experienced larger dislocations toward the inner bulk region than other TMs. The atomic size of TMs should also be paid attention. The larger atomic size (e.g., Sc or Y) hinders the movement toward the bulk region, thus the dislocation of TMs with larger atomic sizes is less obvious (see Fig. 3).

Interestingly, the high-index Mg(10$\bar{1}$3) behaves differently from the low-index Mg(0001) on the relative stability of plane substitution preference. As shown in Table 1, on the low-index Mg(0001) surface, Cd is the only TM which prefers substitution on Plane A. On the high-index Mg(10$\bar{1}$3) surface, Ni, Cu, Zn, Ag, Cd and Au have a higher stability of Site A1 substitution. Moreover, Ni, Zn, Ag, Cd and Au substitutions are exothermic. It indicates that the high-index Mg(10$\bar{1}$3) is capable of thermodynamically stabilizing these TM catalysts on the outermost surface, which possibly enhances the catalyzing effect. In details, the less even Mg atomic distribution on high-index Mg(10$\bar{1}$3) results in a larger amount of atomic relaxation influenced by charge smoothing and depletion which are more apparent than low-index surfaces [54]. The larger amount of charge depletion in the surface region on high-index Mg(10$\bar{1}$3) induces the lower electron density in the surface region

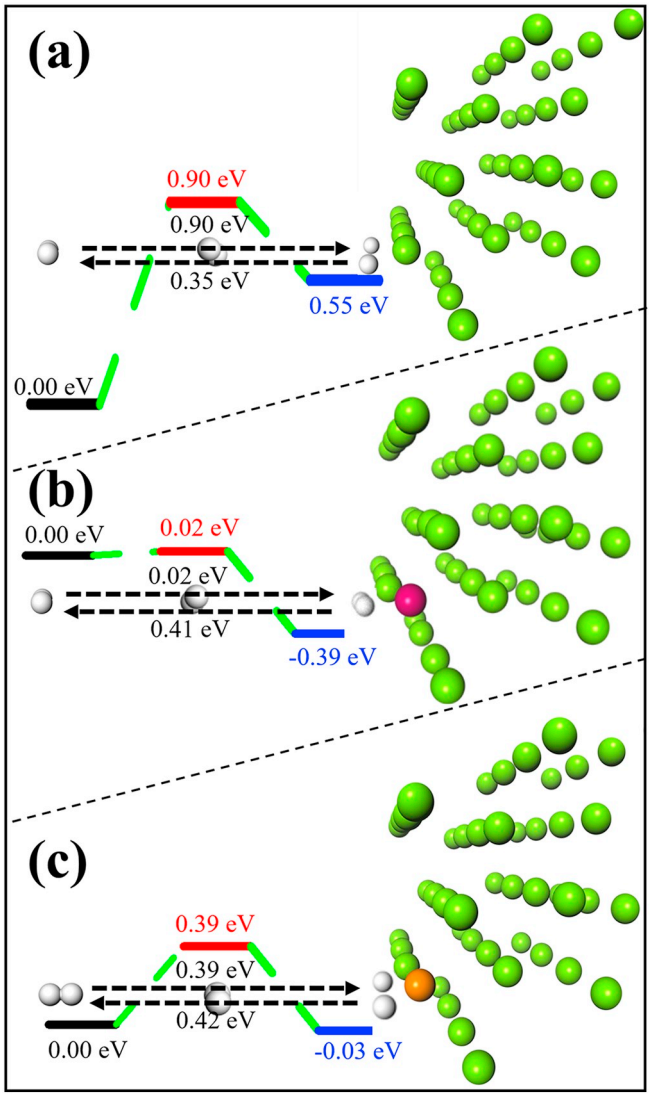

Fig. 6. Minimum energy path (MEP) of H_2 dissociation and formation on (a) pure Mg(10$\bar{1}$3), (b) Ni-substituted Mg(10$\bar{1}$3) and (c) Zn-substituted Mg(10$\bar{1}$3).

Table 3
Comparison of H_2 dissociation and formation barrier of pure Mg and Ni-substituted Mg surface.

Surface	Energy barrier (eV)	
	H_2 dissociation	H_2 formation
Pure Mg(0001) [27]	0.87	0.91
Pure Mg(0001) [41]	0.87	–
Pure Mg(0001) [43]	1.05	c.a. 0.90[b]
Pure Mg(0001) [32]	0.897	c.a. 0.90[b]
Pure Mg(0001) [23]	0.97	c.a. 0.85[b]
Pure Mg(0001) [29]	1.42	c.a. 1.44[b]
Pure Mg(0001)[a]	0.85	0.91
Pure Mg(10$\bar{1}$3)[a]	0.90	0.35
Ni-substituted Mg(0001) [38]	0.06	0.72
Ni-substituted Mg(0001) [23]	0.124	c.a. 0.32[b]
Ni-substituted Mg(0001) [41]	0.06	0.72
Ni-substituted Mg(10$\bar{1}$3)[a]	0.02	0.41

[a] This work.
[b] Evaluated from the figure.

which includes the first and the second outermost surfaces. These two outermost surfaces have a smaller difference between charge density on the high-index Mg(10$\bar{1}$3) than the low-index Mg(0001), leading to a possibility of larger thermodynamic advantage of outermost surface substitution.

In Fig. 3, the comparisons between the dislocations of TMs along *z* direction on the high-index Mg(10$\bar{1}$3) and the low-index Mg(0001). Due to its more obvious charge depletion, the atomic displacement of substituted TMs toward the bulk region along the *z* direction on the high-index Mg(10$\bar{1}$3) is generally larger. It is also found that Sc and Y may have difficulties of moving toward the bulk region because of their larger radii (i.e., 1.6 Å of Sc and 1.80 Å of Y) than Mg radius [55]. On the high-index Mg(10$\bar{1}$3) surface, it is more likely for them to move toward the bulk region, as reflected by their points closer to the black dashed line in Fig. 3.

3.2. H adsorption on TM-substituted Mg surface

For investigating the interaction between TM-substituted surface and H adsorbed, the adsorption energies are calculated and shown in Fig. 4 (the total energies are listed in Table S4). It is found that, in Fig. 4, H adsorption is more energetically favorable when TM substitution takes place at Plane A rather than Plane B of Mg(0001), except for Ag, Cd and Au, indicating that the facilitation of TM-H bond on H adsorption. It is useful to promote the TM to energetically preferentially substitute the outmost Mg [22,23].

In the high-index Mg(10$\bar{1}$3) case, we mainly consider TM substitution sites where TM-H bonds can form (i.e., Site A1 and B1). Fig. 4b delineates the influence on H adsorption energy of TM-H Mg(10$\bar{1}$3). Their trends of E_{ad} are similar to those on Mg(0001) Plane A. Most TM-H interactions lead E_{ad} to be well below the pure Mg surface case (i.e., the black dash line) and the E_{ad} values of the Mg(0001) case shown in Fig. 4a. Interestingly, the stronger TM-H bonds on the high-index Mg (10$\bar{1}$3) can also be manifested in their shorter bond lengths of optimized structures shown in Table 2. Moreover, the two possible substitution sites (Site A and Site B) on the high-index Mg(10$\bar{1}$3) may be more beneficial for the formation of TM-H bonds. However, Cu, Zn, Ag, Cd and Au are not capable of strengthening H adsorption, compared to the pure Mg surface. Our theoretical finding is in agreement with a pervious experimental finding where Mg-Cd alloy is tremendously difficult to activate H_2 [56]. Additionally, several metals with short TM-H bond length have been proved to be experimentally able to lower the hydrogenation temperature, such as Ni [57], Ru [58], Rh [59], Pd [60] and Pt [61]. Briefly, we find that TM-H bond lengths are shorter and the bonds are stronger on Mg(10$\bar{1}$3). TM substitution can play an important role of surface property modification, which can facilitate H adsorption and may contribute to precipitate the H_2 dissociation and H diffusion.

3.3. H_2 dissociation and formation on Ni- and Zn- substituted Mg(10$\bar{1}$3) surface

We have discussed the stabilities of the TM-substituted Mg(0001) and Mg(10$\bar{1}$3) surface, and the interactions between the surface and the adsorbed H. Expectantly, one or few inexpensive metals could preferentially and stably substitute the Mg atom on the surface and through which could dramatically decrease related energy barriers during H uptake and release. To fulfill the mentioned requirement, the metals should (i) have a negative and lower E_{sub} at the outermost layer than the inner layer; and (ii) enhance the bonding between H and TM-doped Mg surface. On the Mg(0001), Cd is more energetically favorable to replace Mg at Plane A, but it is difficult to form a bond with H. Unfortunately, no TM can preferentially and stably replace on Plane A. For Mg(10$\bar{1}$3) surface, Ni, Zn, Ag, Cd and Au satisfy the condition (i) i.e., these TMs are able to stably substitute at the outmost surface. Moreover, Ni, Zn, Ag and Au significantly strengthen the H bonding with the surface compared to pure Mg(10$\bar{1}$3) surface (Table 2), implying the potentials of which improve the H kinetics sorption. Among them, Ag and Au are noble metals with high molar masses (107.9 and 197.0 g/mol) that burden the hydrogen content of the hydride, whereas

Ni and Zn are low-cost and abundant on earth and can be our investigation representatives.

Fig. 5a plots the charge density of the Ni/Mg(10$\bar{1}$3) surface, which corresponds to the projected density of state (PDOS) in Fig. 5b. Bader Charge Analysis [62,63] shows a surface electron accumulation of 13.4 *e* to Ni the source of which is from adjacent Mg atoms. Fig. 5c depicts the charge density difference of the H adsorbed Ni/Mg(10$\bar{1}$3). The adsorption of H, directly bonded to Ni atom, is mainly affected by Ni. An electron transfer from Ni to H can be observed. We compare the PDOS of Ni/Mg(10$\bar{1}$3) before and after H adsorption (Fig. 5b and d). H 1*s* mainly hybridizes with Ni 3*s*, while its interaction with Mg, Ni 3*p* and Ni 3*d* is much weaker. Ni 3*d* barely has no interaction with H 1*s* in Ni/Mg(10$\bar{1}$3). However, the case of Zn/Mg(10$\bar{1}$3) is different. The Zn 3*d* weakly hybridizes with H 1*s* at around −7.5 eV, while Mg 2*s* slightly overlaps with H 1*s* near −6.5 eV, suggesting that Ni 3*d* and Mg 2*s* contribute to H adsorption. The charge density difference in Fig. 5g illustrates that charge depletion occurs in an area around Zn much broader than that in Ni/Mg(10$\bar{1}$3) case in Fig. 5c, indicating that the interaction between H and Mg in Zn/Mg(10$\bar{1}$3) is stronger than that between H and Ni/Mg(10$\bar{1}$3).

The H_2 dissociations and formations on Ni- and Zn-substituted Mg (10$\bar{1}$3) are respectively considered and their reaction pathways and energy barriers are fully considered with comparison with the pure Mg (10$\bar{1}$3) surface case. Fig. 6 shows the minimum energy path (MEP) of three types of Mg surface. Consistency between dissociation and formation of H_2 are carefully checked. H_2 adsorption is strong endothermic, strong exothermal and week exothermal on pure Mg(10$\bar{1}$3), Ni/Mg(10$\bar{1}$3) and Zn/Mg(10$\bar{1}$3), whereas the formation process on each surface is opposite to that. NEB results show that the H_2 dissociation barrier on pure Mg(10$\bar{1}$3) is 0.90 eV, while the ones on pure Mg(0001) are 0.85 eV (this study), and more details are listed in Table 3. Ni/Mg (10$\bar{1}$3) significantly decreases the H_2 dissociation barrier to 0.02 eV, while Zn/Mg(10$\bar{1}$3) reduces the dissociation barrier to 0.39 eV. For the H_2 formation, these two TM-substituted surfaces have energy barriers of 0.41 eV and 0.42 eV, slightly more than the pure Mg(10$\bar{1}$3) case of 0.35 eV. To the best of our knowledge, hydrogen dissociation on Zn-substituted Mg(0001) surface has not been explored. The comparison of energy barriers in Table 3 implies the advantage of H_2 formation on Mg (10$\bar{1}$3) compared to Mg(0001) surface. In brief, compared to pure high-index Mg(10$\bar{1}$3) surface, the TM-substituted surfaces have a much lower H_2 dissociation energy barrier and a similar H_2 formation energy barrier. These TM-substituted surfaces may lead to an obvious lowering of experimental hydrogenation and dehydrogenation temperatures.

4. Conclusion

We conduct systematic DFT calculations to study the stability of substituted transition metals substituted Mg(0001) and Mg(10$\bar{1}$3) surfaces and their interactions with hydrogen. Most transition metals (Sc, Ti, V, Cr, Mn, Fe, Co, Ni, Cu, Zn, Y, Zr, Nb, Mo, Tc, Ru, Rh, Pd, Ag, Pt, Au), except for Cd, are more stable to be substituted at the second Mg layer (Plane B) on Mg(0001), while Ni, Zn, Ag, Cd, and Au are capable of exothermically stably replacing outermost Mg on Mg(10$\bar{1}$3). We attribute these stable substitutions to the greater amount of charge depletion on the high-index surface. Consequently, more obvious displacement of TMs toward the *z* direction can be observed. Moreover, TM-H bonding is stronger on the high-index Mg(10$\bar{1}$3) surface than on the conventional Mg(0001) surface, which facilitates H_2 dissociation and H diffusion. Considering the substitution stability, contribution to H adsorption and transition metal availability, Ni/Mg(10$\bar{1}$3) and Zn/Mg (10$\bar{1}$3) are chosen to be the representatives. The NEB calculation results indicate that both surfaces dramatically reduce H_2 dissociation barrier while having an H_2 formation energy barrier similar to that on the pure Mg(10$\bar{1}$3), which implies the Ni and Zn doping on Mg(10$\bar{1}$3) may induce a decrease in the operation temperature. Combining our results in this study and in our previous investigations that Mg(10$\bar{1}$3) has thermodynamic and kinetic advantages of H adsorption and diffusion over conventional Mg(0001), we consider that the TM-substituted Mg (10$\bar{1}$3), which exhibits better H sorption properties than pure Mg(10$\bar{1}$3), may open a new page for Mg-based hydrogen storage materials, and await related experimental works for digging the hydrogen storage potential of the high-index TM-doped surfaces.

Acknowledgments

This work is financially supported by NSFC (Grant Nos.11574088 and 51621001) and Major Science and Technology Projects of R & D and industrialization of key technologies for Maoming petrochemical industrial chain extension in Guangdong (2012A090300006). The computer times at National Supercomputing Center in Guangzhou (NSCCGZ) is gratefully acknowledged.

Appendix A. Supplementary data

Supplementary data to this article can be found online at https://doi.org/10.1016/j.apsusc.2019.02.124.

References

[1] I.P. Jain, C. Lal, A. Jain, Hydrogen storage in Mg: a most promising material, Int. J. Hydrog. Energy 35 (2010) 5133–5144, https://doi.org/10.1016/j.ijhydene.2009.08.088.
[2] P. Jena, Materials for hydrogen storage: past, present, and future, J. Phys. Chem. Lett. 2 (2011) 206–211, https://doi.org/10.1021/jz1015372.
[3] L. Yan, L. Cao, P. Dai, X. Gu, D. Liu, L. Li, Y. Wang, X. Zhao, Metal-organic frameworks derived nanotube of nickel–cobalt bimetal phosphides as highly efficient electrocatalysts for overall water splitting, Adv. Funct. Mater. 27 (2017) 1–10, https://doi.org/10.1002/adfm.201703455.
[4] N. Jacobson, B. Tegner, E. Schröder, P. Hyldgaard, B.I. Lundqvist, Hydrogen dynamics in magnesium and graphite, Comput. Mater. Sci. 24 (2002) 273–277, https://doi.org/10.1016/S0927-0256(02)00175-1.
[5] P. Chen, Z. Xiong, J. Luo, J. Lin, K. Lee Tan, Interaction of hydrogen with metal nitrides and imides, Nature (2002), https://doi.org/10.1038/nature01210.
[6] R. Mohtadi, M. Matsui, T.S. Arthur, S.J. Hwang, Magnesium borohydride: From hydrogen storage to magnesium battery, Angew. Chem. Int. Ed. 51 (2012) 9780–9783, https://doi.org/10.1002/anie.201204913.
[7] P. Selvam, B. Viswanathan, C.S. Swamy, V. Srinivasan, Magnesium and magnesium alloy hydrides, Int. J. Hydrog. Energy 11 (1986) 169–192, https://doi.org/10.1016/0360-3199(86)90082-0.
[8] Y. Sun, C. Shen, Q. Lai, W. Liu, D.W. Wang, K.F. Aguey-Zinsou, Tailoring magnesium based materials for hydrogen storage through synthesis: current state of the art, Energy Storage Mater. 10 (2018) 168–198, https://doi.org/10.1016/j.ensm.2017.01.010.
[9] Y.S. Au, M. Ponthieu, R. Van Zwienen, C. Zlotea, F. Cuevas, K.P. De Jong, P.E. De Jongh, Synthesis of Mg2Cu nanoparticles on carbon supports with enhanced hydrogen sorption kinetics, J. Mater. Chem. A 1 (2013) 9983–9991, https://doi.org/10.1039/c3ta10926g.
[10] M. Ponthieu, F. Cuevas, J.F. Fernández, L. Laversenne, F. Porcher, M. Latroche, Structural properties and reversible deuterium loading of MgD2–TiD2 nanocomposites, J. Phys. Chem. C 117 (2013) 18851–18862, https://doi.org/10.1021/jp405803x.
[11] Q. Li, Y. Li, B. Liu, X. Lu, T. Zhang, Q. Gu, The cycling stability of the in situ formed Mg-based nanocomposite catalyzed by YH_2, J. Mater. Chem. A 5 (2017) 17532–17543, https://doi.org/10.1039/C7TA04551D.
[12] J. Matsuda, K. Yoshida, Y. Sasaki, N. Uchiyama, E. Akiba, In situ observation on hydrogenation of Mg-Ni films using environmental transmission electron microscope with aberration correction, Appl. Phys. Lett. 105 (2014), https://doi.org/10.1063/1.4894101.
[13] F.P. Luo, H. Wang, L.Z. Ouyang, M.Q. Zeng, J.W. Liu, M. Zhu, Enhanced reversible hydrogen storage properties of a Mg-In-Y ternary solid solution, Int. J. Hydrog. Energy 38 (2013) 10912–10918, https://doi.org/10.1016/j.ijhydene.2013.03.007.
[14] V. Yartys, R. Denys, Structure–properties relationship in RE 3 − x Mg x Ni 9 H 10 – 13 (RE = La,Pr,Nd) hydrides for energy storage, J. Alloys Compd. 645 (2015) S412–S418, https://doi.org/10.1016/j.jallcom.2014.12.091.
[15] Y. Li, Q. Gu, Q. Li, T. Zhang, In-situ synchrotron X-ray diffraction investigation on hydrogen-induced decomposition of long period stacking ordered structure in Mg–Ni–Y system, Scr. Mater. 127 (2017) 102–107, https://doi.org/10.1016/j.scriptamat.2016.09.011.
[16] Y.T. Wang, C.B. Wan, R.L. Wang, X.H. Meng, X. Ju, Synchrotron EXAFS studies of Ti-doped Mg2Ni alloy on the cycling behavior, Int. J. Hydrog. Energy 39 (2014) 13824–13831, https://doi.org/10.1016/j.ijhydene.2014.03.042.
[17] A. Zaluska, L. Zaluski, J.O. Ström-Olsen, Nanocrystalline magnesium for hydrogen storage, J. Alloys Compd. 288 (1999) 217–225, https://doi.org/10.1016/S0925-8388(99)00073-0.
[18] C. Shen, K.F. Aguey-Zinsou, Can γ-MgH2improve the hydrogen storage properties of

magnesium, J. Mater. Chem. A 5 (2017) 8644–8652, https://doi.org/10.1039/c7ta01724c.
[19] L. Ouyang, J. Tang, Y. Zhao, H. Wang, X. Yao, J. Liu, J. Zou, M. Zhu, Express penetration of hydrogen on Mg(1013) along the close-packed-planes, Sci. Rep. 5 (2015) 1–9, https://doi.org/10.1038/srep10776.
[20] C. Chiu, A.M. Yang, High-temperature hydrogen cycling properties of magnesium-based composites, Mater. Lett. 169 (2016) 144–147, https://doi.org/10.1016/j.matlet.2016.01.103.
[21] J.A. Puszkiel, P. Arneodo Larochette, A. Baruj, G. Meyer, F.C. Gennari, Hydrogen cycling properties of xMg-Fe materials (x: 2, 3 and 15) produced by reactive ball milling, Int. J. Hydrog. Energy 41 (2016) 1688–1698, https://doi.org/10.1016/j.ijhydene.2015.10.140.
[22] M. Chen, X.B. Yang, J. Cui, J.J. Tang, L.Y. Gan, M. Zhu, Y.J. Zhao, Stability of transition metals on Mg(0001) surfaces and their effects on hydrogen adsorption, Int. J. Hydrog. Energy 37 (2012) 309–317, https://doi.org/10.1016/j.ijhydene.2011.09.065.
[23] S. Banerjee, C.G.S. Pillai, C. Majumder, First-principles study of the H2 interaction with transition metal (Ti, V, Ni) doped Mg(0001) surface: implications for H-storage materials, J. Chem. Phys. 129 (2008) 174703, https://doi.org/10.1063/1.3000673.
[24] D.M. Bird, L.J. Clarke, M.C. Payne, I. Stich, Dissociation of H2 on Mg(0001), Chem. Phys. Lett. 212 (1993) 518–524, https://doi.org/10.1016/0009-2614(93)87239-Y.
[25] T. Vegge, Locating the rate-limiting step for the interaction of hydrogen with Mg (0001) using density-functional theory calculations and rate theory, Phys. Rev. B 70 (2004) 1–7, https://doi.org/10.1103/PhysRevB.70.035412.
[26] A.J. Du, S.C. Smith, X.D. Yao, G.Q. Lu, Catalytic effects of subsurface carbon in the chemisorption of hydrogen on a Mg(0001) surface: an ab-initio study, J. Phys. Chem. B 110 (2006) 1814–1819, https://doi.org/10.1021/jp055972d.
[27] M. Pozzo, D. Alfè, Hydrogen dissociation on Mg(0001) studied via quantum Monte Carlo calculations, Phys. Rev. B 78 (2008) 1–5, https://doi.org/10.1103/PhysRevB.78.245313.
[28] M. Pozzo, D. Alfè, The role of steps in the dissociation of H2 on Mg(0001), J. Phys. Condens. Matter 21 (2009), https://doi.org/10.1088/0953-8984/21/9/095004.
[29] Z. Han, H. Chen, S. Zhou, Dissociation and diffusion of hydrogen on defect-free and vacancy defective Mg (0001) surfaces: a density functional theory study, Appl. Surf. Sci. 394 (2017) 371–377, https://doi.org/10.1016/j.apsusc.2016.10.101.
[30] Y. Li, P. Zhang, B. Sun, Y. Yang, Y. Wei, Atomic hydrogen adsorption and incipient hydrogenation of the Mg(0001) surface: a density-functional theory study, J. Chem. Phys. 131 (2009) 034706, https://doi.org/10.1063/1.3182851.
[31] T. Jiang, L.X. Sun, W.X. Li, First-principles study of hydrogen absorption on Mg (0001) and formation of magnesium hydride, Phys. Rev. B 81 (2010) 1–9, https://doi.org/10.1103/PhysRevB.81.035416.
[32] H. Lei, C. Wang, Y. Yao, Y. Wang, M. Hupalo, D. McDougall, M. Tringides, K. Ho, Strain effect on the adsorption, diffusion, and molecular dissociation of hydrogen on Mg (0001) surface, J. Chem. Phys. 139 (2013), https://doi.org/10.1063/1.4839595.
[33] J. Xin, J. Wang, Y. Du, L. Sun, B. Huang, Site preference and diffusion of hydrogen during hydrogenation of Mg: a first-principles study, Int. J. Hydrog. Energy 41 (2016) 3508–3516, https://doi.org/10.1016/j.ijhydene.2015.12.157.
[34] J.J. Tang, X.B. Yang, M. Chen, M. Zhu, Y.J. Zhao, First-principles study of biaxial strain effect on hydrogen adsorbed Mg (0001) surface, J. Phys. Chem. C 116 (2012) 14943–14949, https://doi.org/10.1021/jp303480c.
[35] P. Vajeeston, P. Ravindran, A. Kjekshus, H. Fjellvåg, Pressure-induced structural transitions in MgH_2, Phys. Rev. Lett. 89 (2002) 175506, https://doi.org/10.1103/PhysRevLett.89.175506.
[36] P. Vajeeston, P. Ravindran, B.C. Hauback, H. Fjellvåg, A. Kjekshus, S. Furuseth, M. Hanfland, Structural stability and pressure-induced phase transitions in MgH_2, Phys. Rev. B 73 (2006) 1–8, https://doi.org/10.1103/PhysRevB.73.224102.
[37] J.J. Tang, X.B. Yang, L. Ouyang, M. Zhu, Y.J. Zhao, A systematic first-principles study of surface energies, surface relaxation and Friedel oscillation of magnesium surfaces, J. Phys. D. Appl. Phys. 47 (2014) 115305, https://doi.org/10.1088/0022-3727/47/11/115305.
[38] M. Pozzo, D. Alfè, Hydrogen dissociation and diffusion on transition metal (=Ti, Zr, V, Fe, Ru, Co, Rh, Ni, Pd, Cu, Ag)-doped Mg(0001) surfaces, Int. J. Hydrog. Energy (2009), https://doi.org/10.1016/j.ijhydene.2008.11.109.
[39] A.J. Du, S.C. Smith, X.D. Yao, G.Q. Lu, First-principle study of adsorption of hydrogen on Ti-doped Mg(0001) surface, J. Phys. Chem. B 110 (2006) 21747–21750, https://doi.org/10.1021/jp063286o.
[40] A.J. Du, S.C. Smith, X.D. Yao, G.Q. Lu, Hydrogen spillover mechanism on a Pd-doped Mg surface as revealed by ab initio density functional calculation, J. Am. Chem. Soc. 129 (2007) 10201–10204, https://doi.org/10.1021/ja0722776.
[41] M. Pozzo, D. Alfè, A. Amieiro, S. French, A. Pratt, Hydrogen dissociation and diffusion on Ni- and Ti-doped Mg(0001) surfaces, J. Chem. Phys. 128 (2008) 094703, https://doi.org/10.1063/1.2835541.
[42] J.G. Du, X.Y. Sun, G. Jiang, A DFT study on small M-doped titanium (M = V, Fe, Ni) clusters: structures, chemical bonds and magnetic properties, Eur. Phys. J. D 55 (2009) 111–120, https://doi.org/10.1140/epjd/e2009-00177-6.
[43] A.J. Du, S.C. Smith, X.D. Yao, G.Q. Lu, The role of Ti as a catalyst for the dissociation of hydrogen on a Mg(0001) surface, J. Phys. Chem. B 109 (2005) 18037–18041, https://doi.org/10.1021/jp052804c.
[44] H.T. Uchida, S. Wagner, M. Hamm, J. Kürschner, R. Kirchheim, B. Hjörvarsson, A. Pundt, Absorption kinetics and hydride formation in magnesium films: effect of driving force revisited, Acta Mater. 85 (2015) 279–289, https://doi.org/10.1016/j.actamat.2014.11.031.
[45] G. Kresse, J. Furthmüller, Efficient iterative schemes for ab initio total-energy calculations using a plane-wave basis set, Phys. Rev. B 54 (1996) 11169–11186, https://doi.org/10.1103/PhysRevB.54.11169.
[46] P.E. Blöchl, Projector augmented-wave method, Phys. Rev. B 50 (1994) 17953–17979, https://doi.org/10.1103/PhysRevB.50.17953.
[47] D. Joubert, From ultrasoft pseudopotentials to the projector augmented-wave method, Phys. Rev. B 59 (1999) 1758–1775, https://doi.org/10.1103/PhysRevB.59.1758.
[48] J. Perdew, K. Burke, M. Ernzerhof, Generalized gradient approximation made simple, Phys. Rev. Lett. 77 (1996) 3865–3868, https://doi.org/10.1103/PhysRevLett.77.3865.
[49] H.E. Swanson, E. Tatge, Standard X-ray diffraction patterns, J. Res. Natl. Bur. Stand. 46 (1951) 318, https://doi.org/10.6028/jres.046.036.
[50] C. Kittel, Introduction to solid state physics, Solid State Phys. 703 (2005), https://doi.org/10.1119/1.1974177.
[51] H.J. Monkhorst, J.D. Pack, Special points for Brillouin-zon integrations, Phys. Rev. B 13 (1976) 5188–5192, https://doi.org/10.1103/PhysRevB.16.1748.
[52] G. Henkelman, H. Jónsson, Improved tangent estimate in the nudged elastic band method for finding minimum energy paths and saddle points, J. Chem. Phys. 113 (2000) 9978–9985, https://doi.org/10.1063/1.1323224.
[53] C. Kittel, Introduction to solid state physics, Am. J. Phys. 21 (1953) 650, https://doi.org/10.1119/1.1933590.
[54] J.S. Lowe, D.J. Siegel, Reaction pathways for solvent decomposition on magnesium anodes, J. Phys. Chem. C 122 (2018) 10714–10724, https://doi.org/10.1021/acs.jpcc.8b01752.
[55] J.A. McCleverty, T.J. Meyer, Comprehensive Coordination Chemistry II, (2004), https://doi.org/10.1016/C2009-1-28216-5.
[56] G. Liang, R. Schulz, The reaction of hydrogen with Mg-Cd alloys prepared by mechanical alloying, J. Mater. Sci. 39 (2004) 1557–1562, https://doi.org/10.1023/B:JMSC.0000016151.51658.08.
[57] J. Zhang, Y. Zhu, X. Zang, Q. Huan, W. Su, D. Zhu, L. Li, Nickel-decorated graphene nanoplates for enhanced H 2 sorption properties of magnesium hydride at moderate temperatures, J. Mater. Chem. A 4 (2016) 2560–2570, https://doi.org/10.1039/C5TA09848C.
[58] I.E. Ertas, M. Gulcan, A. Bulut, M. Yurderi, M. Zahmakiran, Rhodium nanoparticles stabilized by sulfonic acid functionalized metal-organic framework for the selective hydrogenation of phenol to cyclohexanone, J. Mol. Catal. A Chem. (2015), https://doi.org/10.1016/j.molcata.2015.09.025.
[59] H. Zhang, A. Han, K. Okumura, L. Zhong, S. Li, S. Jaenicke, G.K. Chuah, Selective hydrogenation of phenol to cyclohexanone by SiO2-supported rhodium nanoparticles under mild conditions, J. Catal. 364 (2018) 354–365, https://doi.org/10.1016/j.jcat.2018.06.002.
[60] Y. Zhu, G. Yu, J. Yang, M. Yuan, D. Xu, Z. Dong, Biowaste soybean curd residue-derived Pd/nitrogen-doped porous carbon with excellent catalytic performance for phenol hydrogenation, J. Colloid Interface Sci. 533 (2019) 259–267, https://doi.org/10.1016/j.jcis.2018.08.067.
[61] X. Yang, X. Yu, L. Long, T. Wang, L. Ma, L. Wu, Y. Bai, X. Li, S. Liao, Pt nanoparticles entrapped in titanate nanotubes (TNT) for phenol hydrogenation: the confinement effect of TNT, Chem. Commun. (2014), https://doi.org/10.1039/c3cc49331h.
[62] G. Henkelman, A. Arnaldsson, H. Jónsson, A fast and robust algorithm for Bader decomposition of charge density, Comput. Mater. Sci. 36 (2006) 354–360, https://doi.org/10.1016/j.commatsci.2005.04.010.
[63] E. Sanville, S.D. Kenny, R. Smith, G. Henkelman, Improved grid-based algorithm for Bader charge allocation, J. Comput. Chem. 28 (2007) 899–908, https://doi.org/10.1002/jcc.20575.